Supplementary Information

Content

1) Supplementary Figures and Tables

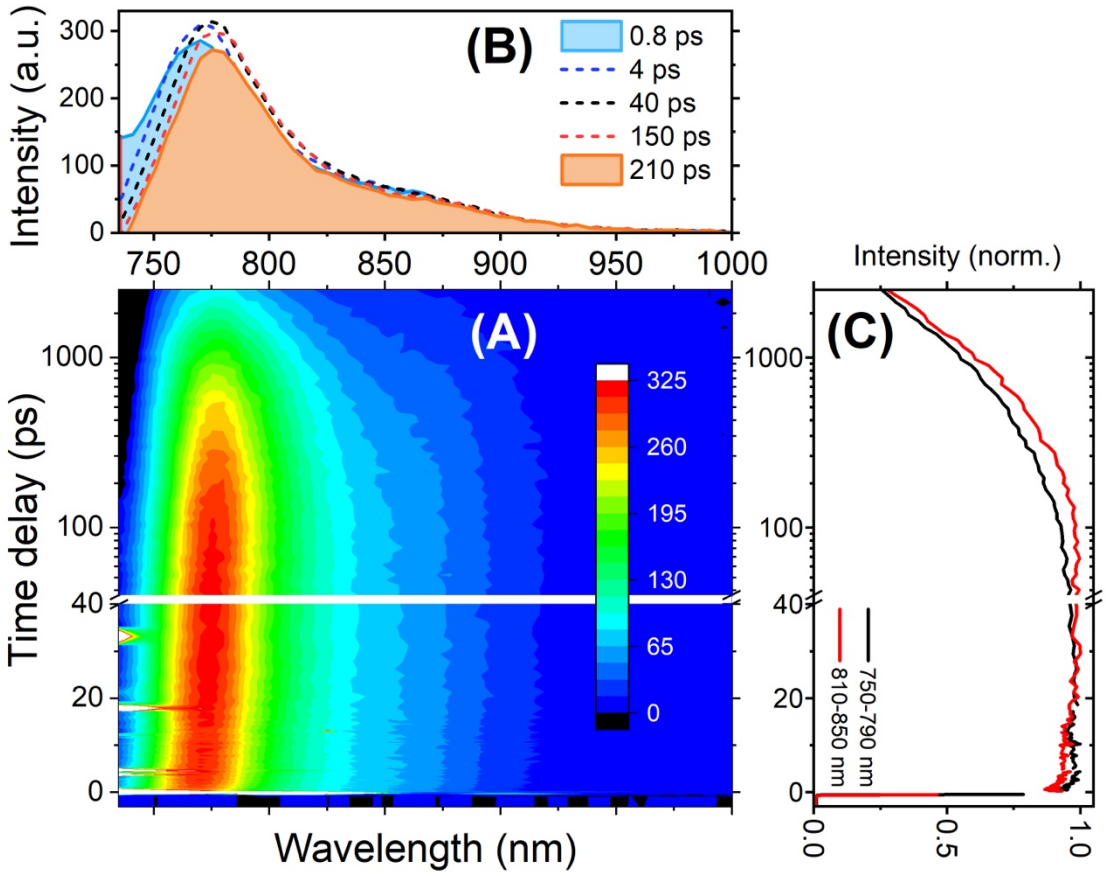

Figure S1. Fluorescence up-conversion data for **TB207** in solution, MA conditions. In addition to the streak camera data (fig. 2), the higher time resolution allows here to obtain evidence for a ≈ 30 ps red-shift due to excited state relaxation. **A)** False color plot of time- and wavelength-resolved emission. **B)** Time-resolved emission spectra for delay times as indicated (dashed lines), the steady-state fluorescence is shown for comparison (orange). **C)** Kinetic traces averaged in wavelength intervals as indicated. The rise time for the long-wavelength kinetics is due to exc. state relaxation.

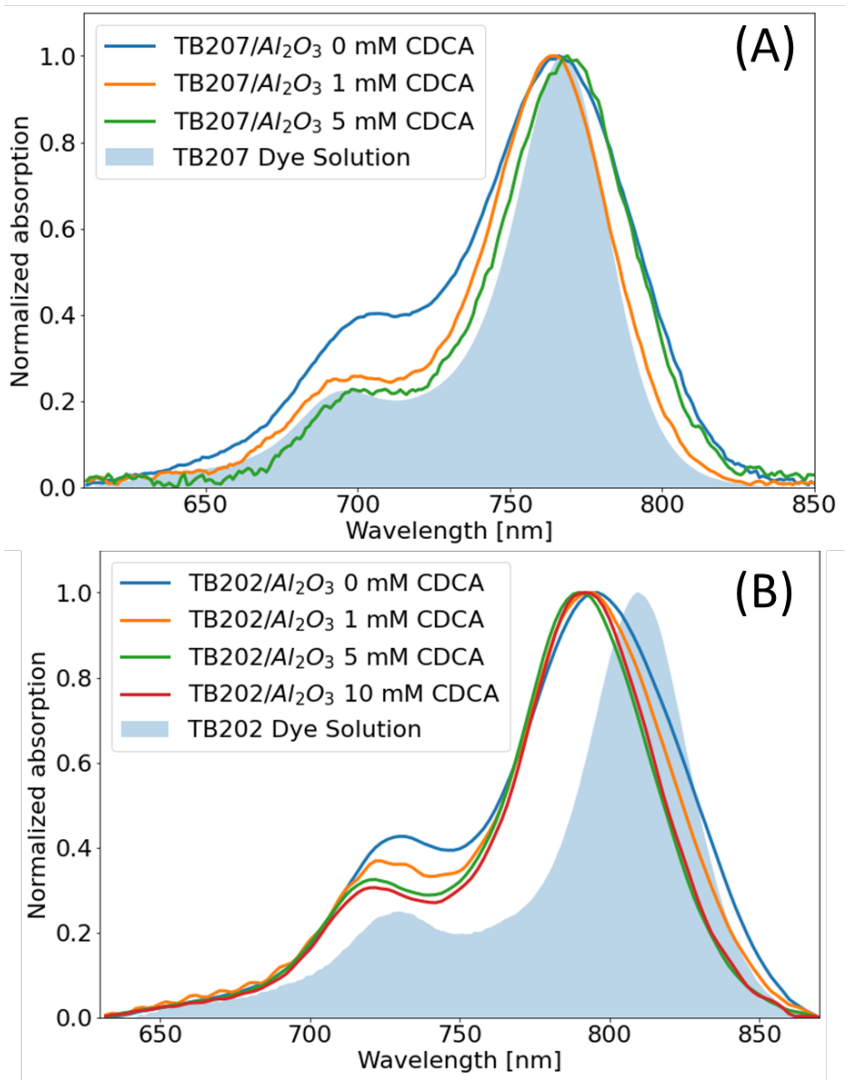

Figure S2. Normalized absorption spectra of TB207 (A) and TB202 (B) Al_2O_3 solar cells. Blue areas are the steady-state absorption spectra of the solution

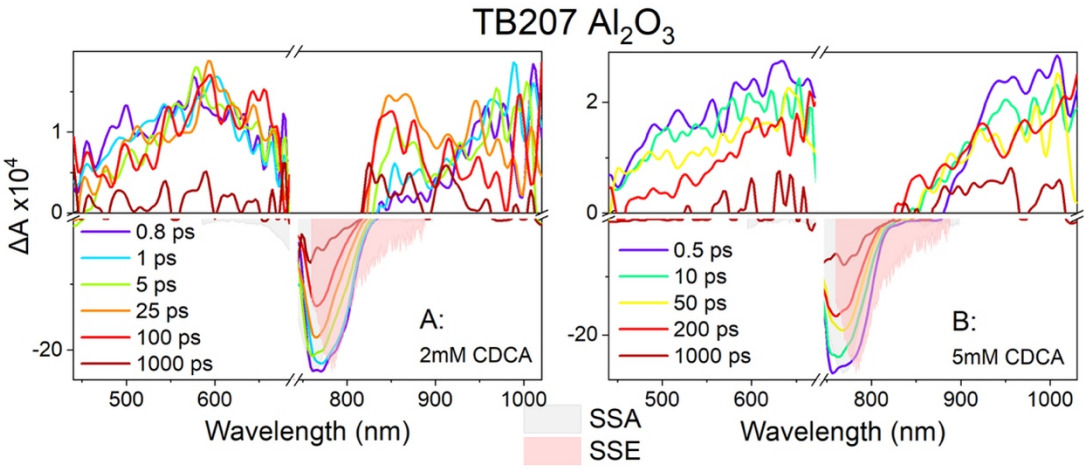

Figure S3. Femtosecond transient absorption for **TB207** on Al_2O_3. **A :** 2 mM CDCA ; **B :** 5mM CDCA. Excitation wavelength 730 nm, Average energy density per pulse 26 μJ/cm^2. Steady-state absorption and emission spectra are plotted sign-inverted as gray and rose areas, respectively.

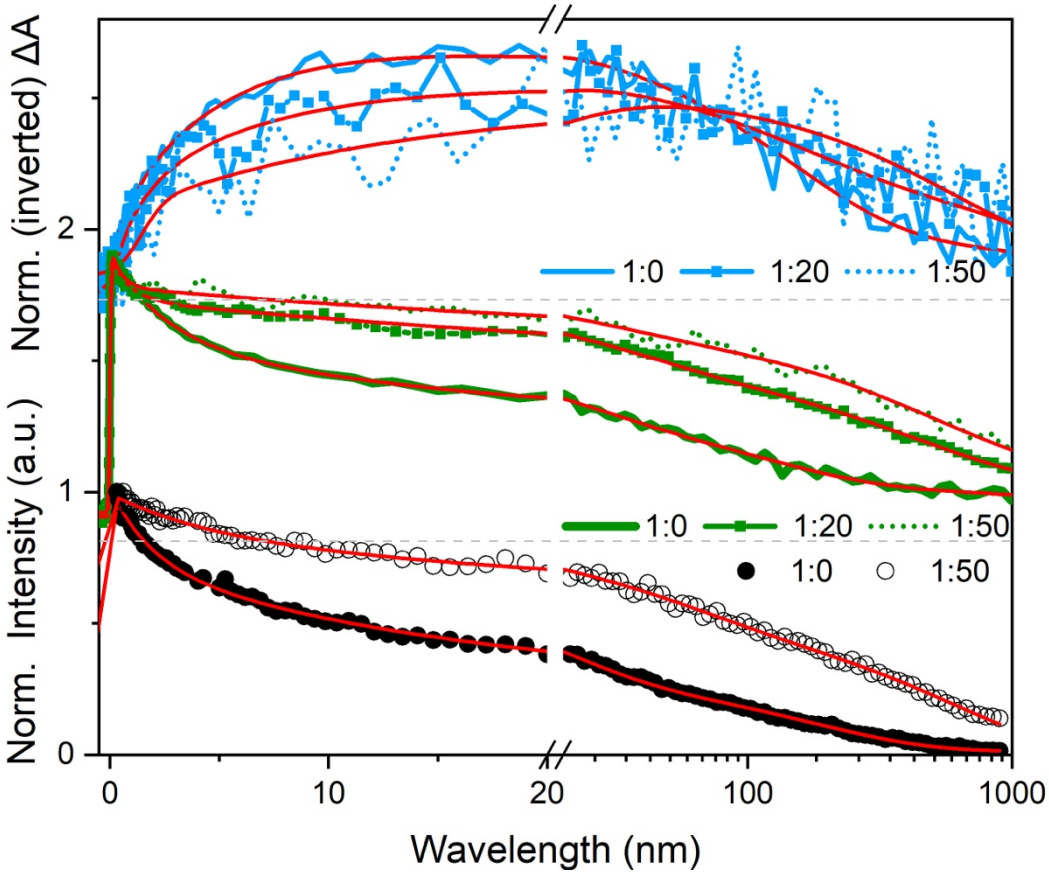

Figure S4. Normalized kinetic traces of transient absorption and fluorescence up-conversion for **TB207**/Al_2O_3 for different CDCA concentrations: 0mM (solid line), 2mM (squares), 5mM (dotted line). Red lines represent the best fits to the data. **Upper panel:** ESA(Agg*) at 880 nm highlighting the progressive ET; **Middle panel:** SE/GSB at 780 nm, plotted with inverted sign. The decay parallels the rise of ESA(Agg*). **Bottom panel:** Fluorescence decay kinetics integrated for ≥ 800 nm. Dots: 0mM CDCA; Open circles: 5mM CDCA. Average energy density per pulse 26 μJ/cm^2.

Table ST1. TB207/Al_2O_3: Results of a 4-components exponential fit for the ESA(Agg*), GSB/SE, and FLUPS kinetics (red lines in fig. S4). Negative amplitudes in the ESA(Agg*) traces characterize the ET time by the rise times of that signal. Conversely, these times appear as decay components in GSB/SE and FLUPS.

The average decay time $<\tau>$ is the arithmetic average, corresponding to a monomer-ensemble average for the ET, as it shows up as SE/GSB and FLUPS decay. Since $\tau 4$ is due to slow-decaying GSB (not SE), it is not taken into account for $<\tau>$GSB.

CDCA conc. (mM)	signal	A_1(%)	τ_1(ps)	A_2(%)	τ_2(ps)	A_3(%)	τ_3(ps)	A_4(%)	τ_4(ps)	$<\tau>$ (ps)
0	ESA(Agg*)	-10	0.8	-71	4.9	76	140	23	3400	-
	SE/GSB	-34	2.6	-25	19	-30	120	-10	3400	47,2
	FLUPS	35	2	39	17	26	180	-	-	54,1
2.0	ESA(Agg*)	-27	1.3	-57	7.2	45	140	55	1800	
	SE/GSB	16	0.9	25	33	34	350	24	2500	167
5.0	ESA(Agg*)	-80	1.4	-63	13	90	620	10	inf	
	SE/GSB	16	0.5	17	26	38	390	31	2500	221
	FLUPS	24	1.8	19	34	57	840	-	-	485

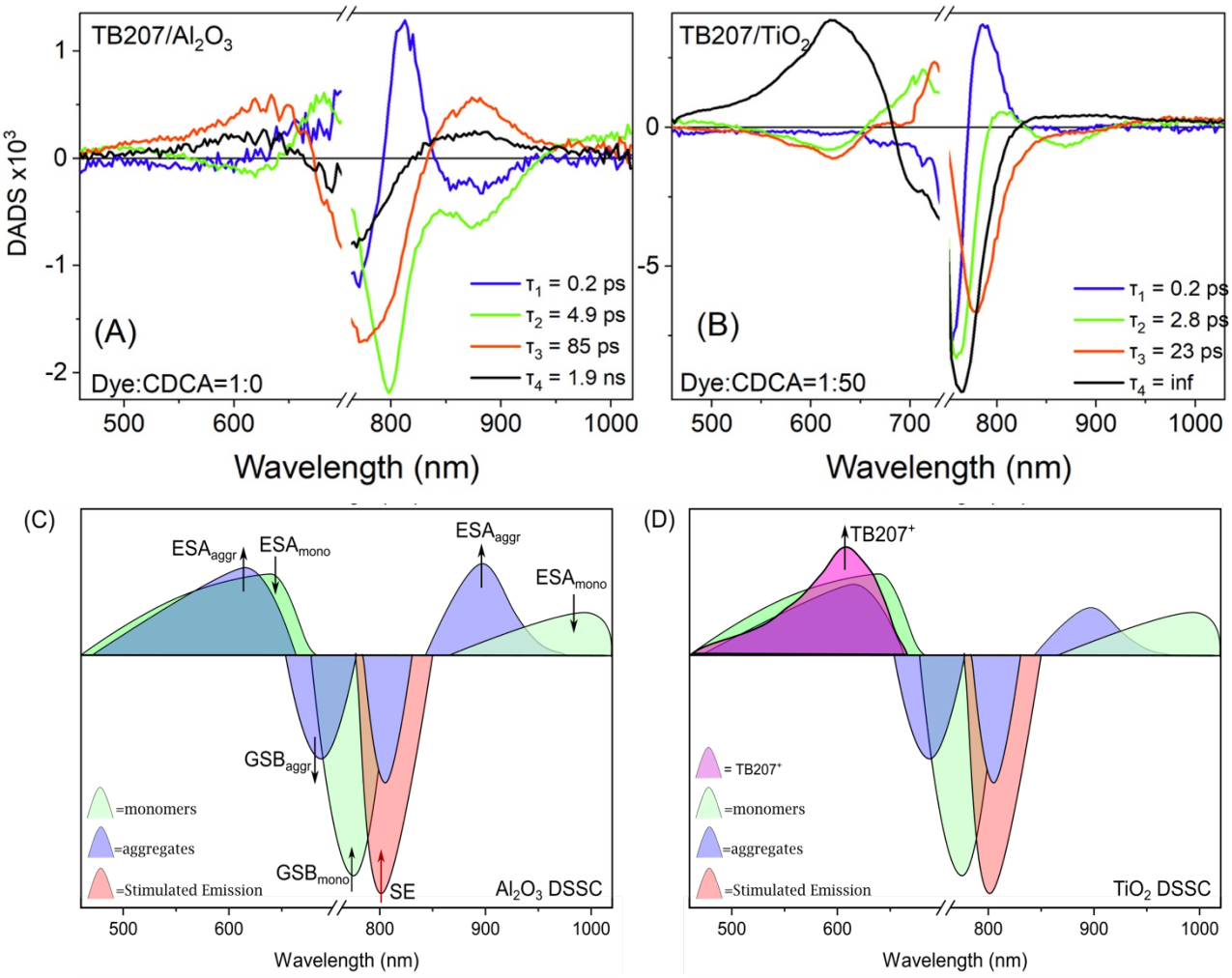

Figure S5. Decay-associated difference spectra and schematic representations of the state-and species specific features in the ΔA signal. **A:** DADS for **TB207**/0mM-CDCA/Al_2O_3; **B:** **TB207**/5mM-CDCA/TiO_2; **C+D:** Schematic of the contributions of monomers and aggregates to the GSB, SE and ESA. TB207+ is the main band of cation absorption. In TiO_2 DSSCs, in addition to the overlaying features present in Al_2O_3 DSSCs, the cation absorption ($TB207^+$) is observed at the same wavelength region as ESA_{aggr} and ESA_{mono}.

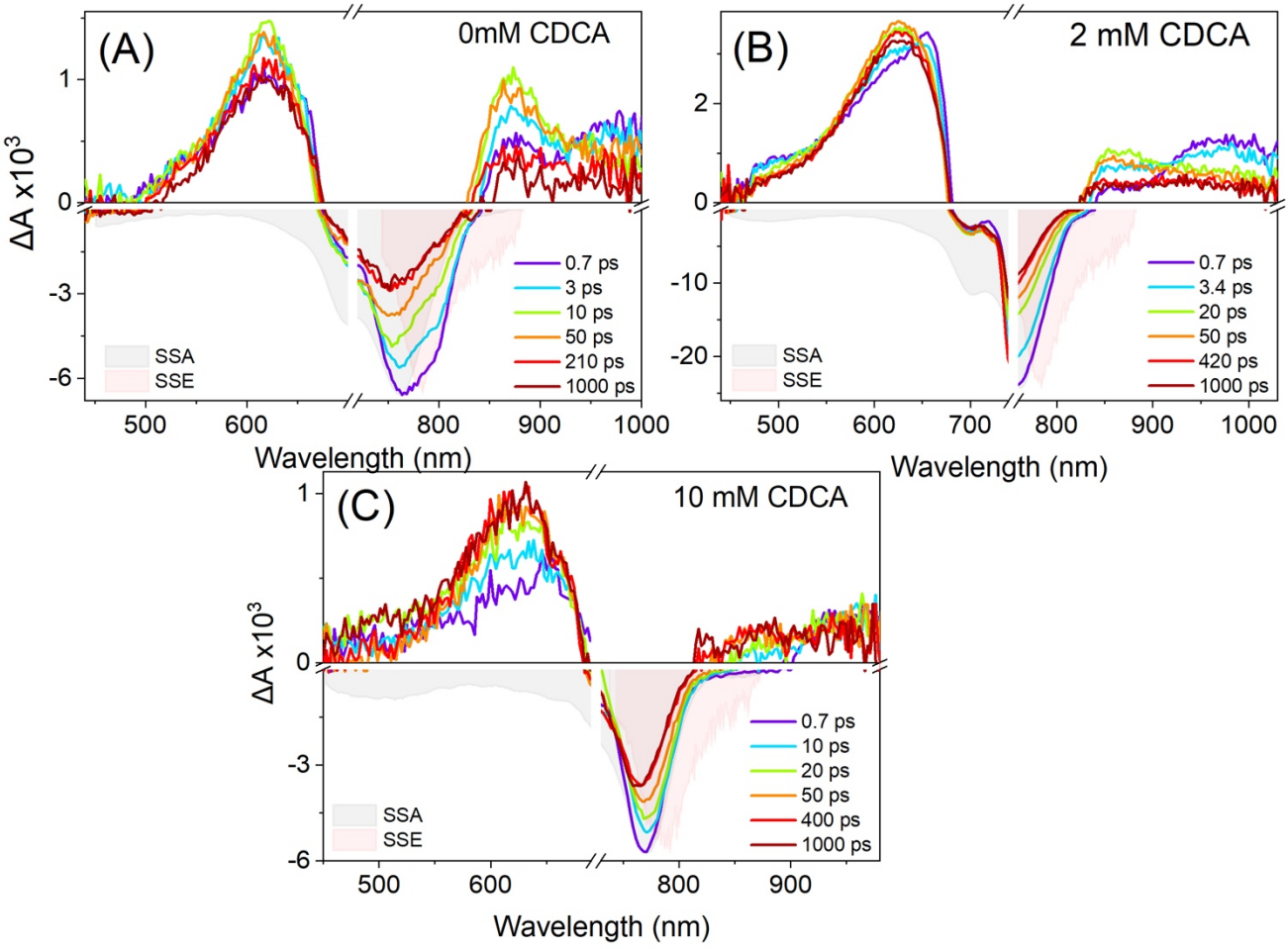

Figure S6. Transient absorption spectra for **TB207**/TiO_2; **A:** 0 mM CDCA; **B:** 2 mM CDCA; **C: 1**0 mM CDCA. The 5 mM data are in fig. 7B in the main text.

Table ST2. TB207/TiO_2: Results of a 4-components exponential fit for the ESA(Agg*), PP(TB207+),GSB/SE, and FLUPS kinetics (solid lines in fig. S7&8). "inf" means a decay time >> 5ns. Negative amplitudes in the ESA(Agg*) and PP(TB207+) traces characterize the ET and CT times by the rise times of that signal. Conversely, these times appear as decay components in GSB/SE and FLUPS. For 0mM CDCA concentration, the ESA in the 600-650 nm range, and at 850-800 nm, are a mix of ESA(Agg*) and TB207+, as indicated by the "inf" time constant (see fig. S5).
GA: Lifetimes obtained from global fitting. The differences with the single wavelength fits indicate the error bar for the GA time constants.
The average decay time <τ> is the arithmetic average, corresponding to a monomer-ensemble average for the ET, as it shows up as SE/GSB and FLUPS decay. The "*" values are the average ET lifetimes obtained from the stretched exponential fits (see main text).

CDCA (mM)	Signal /λ(nm)	A_1(%)	τ_1(ps)	A_2(%)	τ_2(ps)	A_3(%)	τ_3(ps)	A_4(%)	τ_4(ps)	<τ> (ps)
0	ESA(Agg*), 600-630	-15	0.2	-37	3.0	31	130	69	inf	-
	ESA(mono), 650-660	-7	0.5	26	5.9					
	GSB/SE, 780-790	-35	2	-39	17	-26	180	-	-	
	ESA(Agg*), 855-880	-18	0.6	-63	4.8	80	110	20	inf	
	GA		0.3		5.8		76		inf	
	FLUPS	21	1.3	52	6	27	23			9,6±1,5
2.0	600-630	-9	0.8	-21	13	17	430	83	inf	
	ESA(mono), 680-700	-25	2.5	-22	12	43	96	57	Inf	
	GSB/SE, 780-790	44	0.1	-50	6	-26	110	-24	inf	
	ESA(Agg*), 855-880	-32	1.4	-51	6.8	69	96	31	inf	
	GA		0.2		5		52		inf	

5.0	PP(207+), 610-630	-13	1.8	-35	16	5	300	95	inf	
	SE/GSB, 780-780	32	0.2	-47	16	-17	95	35	inf	
	SE/PP(207+), 855-880	-24	1.2	-64	8.7		8.7	38	4.4	
	ESA(mono),950-1000	25	2.4	37	23	11	600	26	inf	
	GA		0.2		2.3		23		inf	
	FLUPS	16	1.5	43	8	41	35			18 ± 2
10.0	PP(207+), 610-630	-9	0.4	-26	11	-32	36	100	inf	
	SE/GSB, 780-780	22	0.6	-46	45	-10	1200	43	Inf	
	SE/PP(207+), 855-880	-6	0.3	-63	9.1	-34	47	60	3.6	
	GA		0.6		8		49			
	FLUPS	13	1.5	42	9.4	45	42			23±3

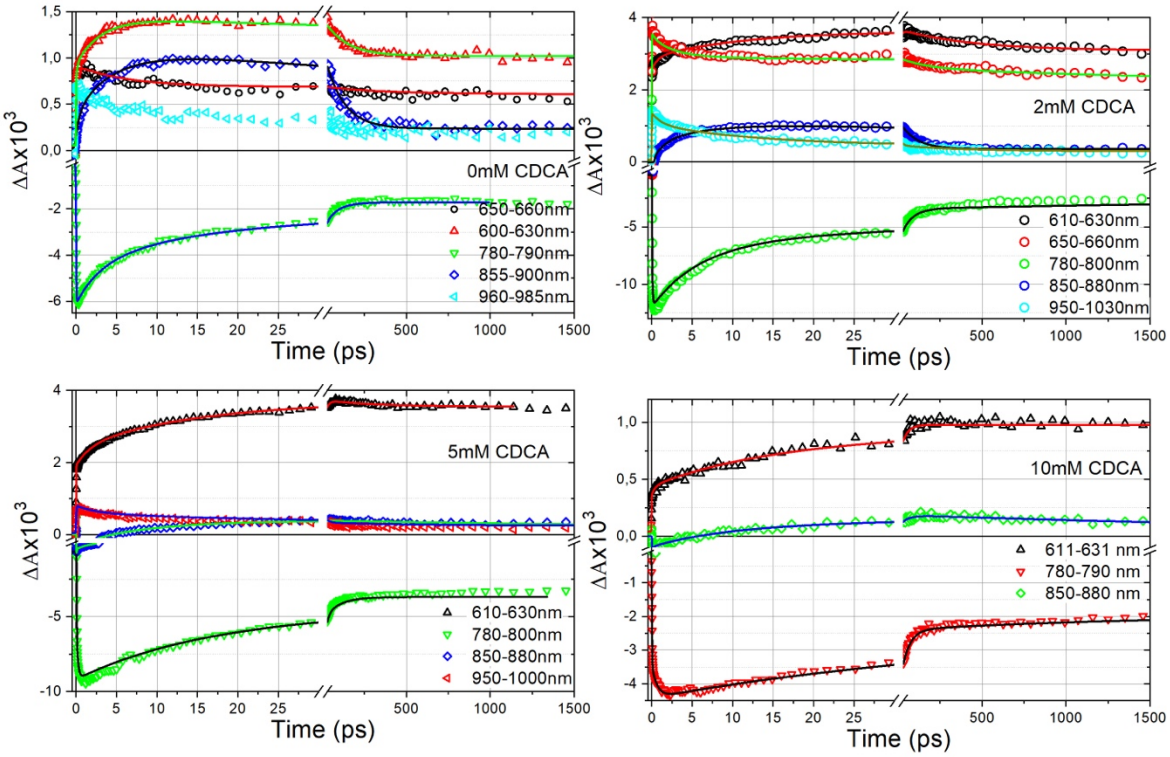

Figure S7. Kinetic traces of TAS **TB207**/TiO_2; **A:** 0 mM CDCA; **B:** 2 mM CDCA; **C:** 5 mM CDCA; **D:** 10 mM CDCA. The solid lines represent 4-exp. fits corresponding to the lifetimes and amplitudes summarized in table **ST2**. Note the break in the time axis at 30 ps and in the different scales of the positive and negative parts of the y-axis.

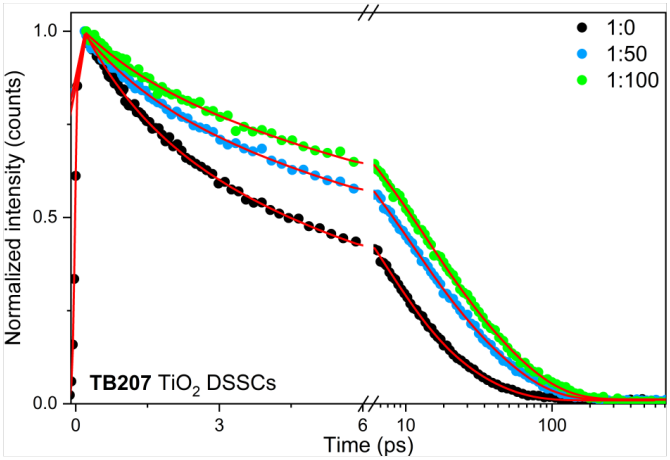

Figure S8. Fluorescence transients of **TB207**/TiO_2, for three different CDCA concentrations. The same devices as in fig. S7. Excitation wavelength 730 nm. Note the break in the time axis at 6ps, and log. scale thereafter.

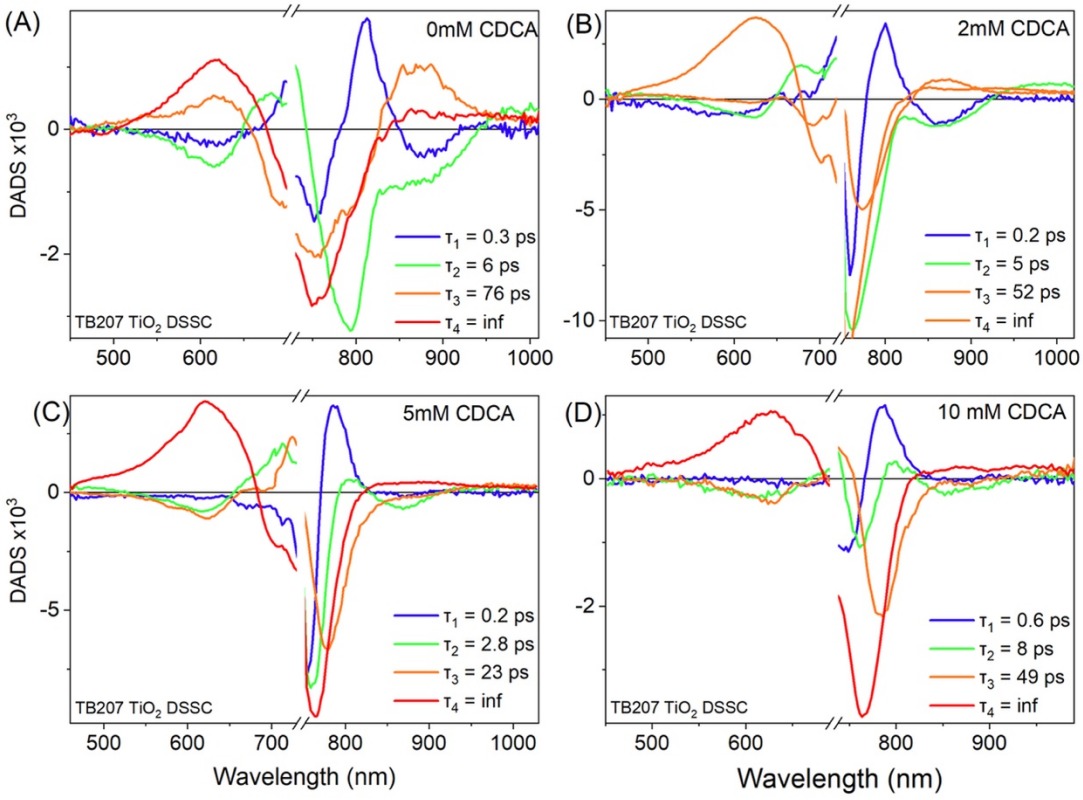

Figure S9. Decay-associated difference spectra for **TB207**/TiO_2; **A:** 0 mM CDCA; **B:** 2 mM CDCA; **C:** 5 mM CDCA; **D:** 20 mM CDCA.

A detailed explanation of DAD spectra: The sub-picosecond component τ_1 mainly displays a red-shift of the SE (neg at 750nm, positive, meaning rise of SE at 790-800 nm). In the case of 0 and 2mM CDCA, the negative component at 550-600nm is most likely a rise of ESA(Agg*), indicating ultrafast ET. This goes in parallel with the positive component at 700-720 nm, attributed to a rise of GSB of the higher energy Agg ground state absorption.

The 3-8 ps component τ_2 is associated with monomer ES decay (ESA > 1000 nm & SE 800-900 nm). In addition, for all CDCA concentrations, the negative component at 880 nm is due to rise of the ESA(Agg*) due to ET, most pronounced for the low CDCA concentrations. This goes along with a weak neg. component at 580-620 nm due to the same process and/or cation formation.

The component τ_3 in the range of tens of ps is associated with ESA(Agg*) decay at 880 nm for the lowest CDCA concentrations. For 5 and 10 mM CDCA it is rather due to SE decay, with a peak at 780 nm. The negative component at 620-640 nm is due to formation of the cation absorption (TB207+).

The infinite time component represents the terminal TAS spectrum representing the cation absorption at 640 nm and a flat weak absorption in the near-IR. This goes along with remaining GSB at 760 nm.

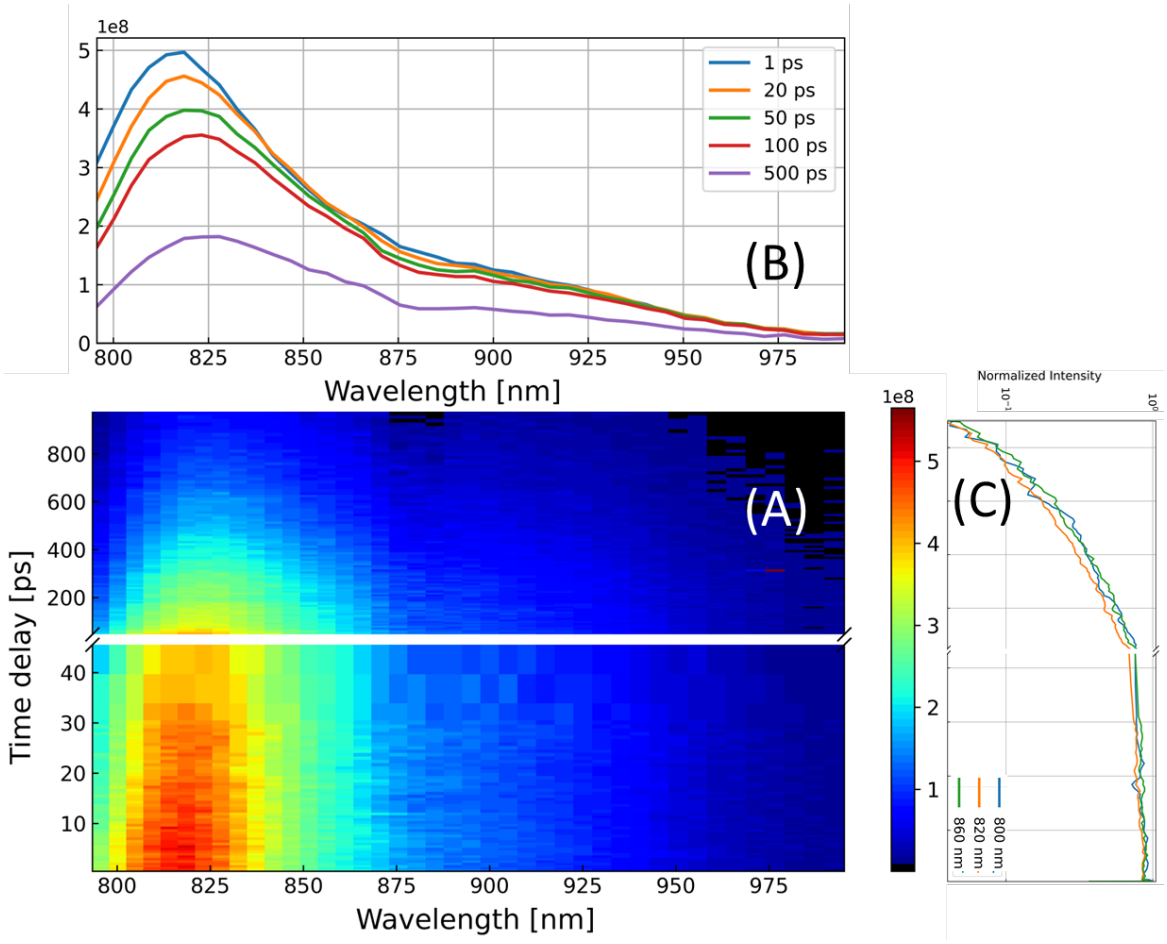

Figure S10. Fluorescence up-conversion data for **TB202** in solution, MA conditions. **A)** False color plot of time- and wavelength-resolved emission. **B)** Time-resolved emission spectra for delay times as indicated **C)** Normalized kinetic traces averaged in wavelength intervals as indicated, plotted on logarithmic scale.

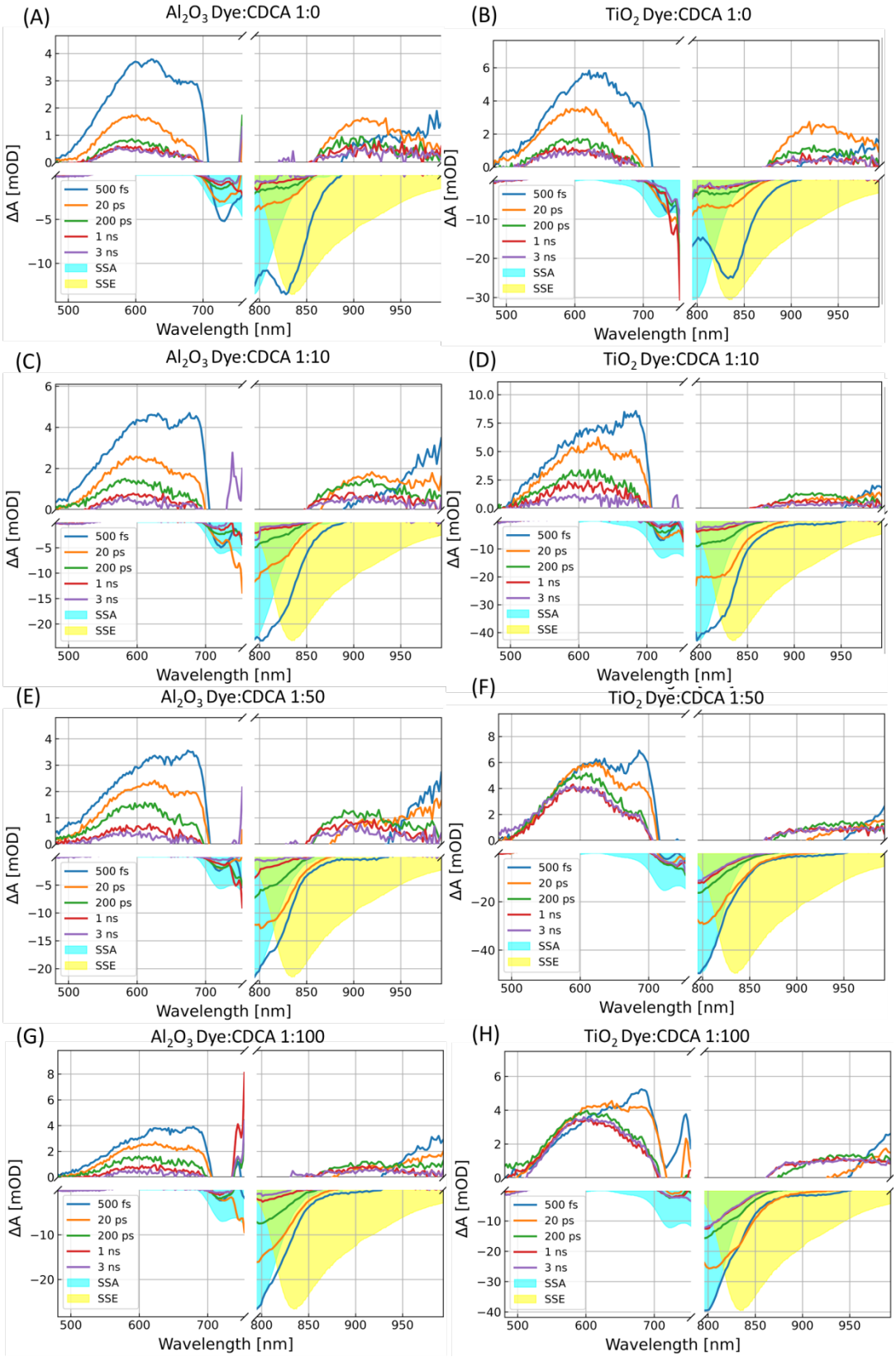

Figure S11. Transient absorption spectra at different time delays for TB202/Al_2O_3 (A,C) and TB202/TiO_2 (B,D) cells. A break on the x-axis was introduced at a wavelength interval; where high pump light scattering occurred masking the signal. For the y-axis different scales are used. The shaded SSA and SSE spectra are the sign-inverted steady-state absorption and fluorescence spectra, which overlap closely to the negative GSB (760-820 nm) and SE signals (>800 nm) respectively. Between 500-700 nm for the $TiIO_2$ (B,DF,H) a non-decaying component appear what we identify as the cation absorption spectrum increasing with the CDCA concentration. In Al_2O_3 (A,C,E,G) due to the high conduction band energy no signature for this photoproduct can be observed.

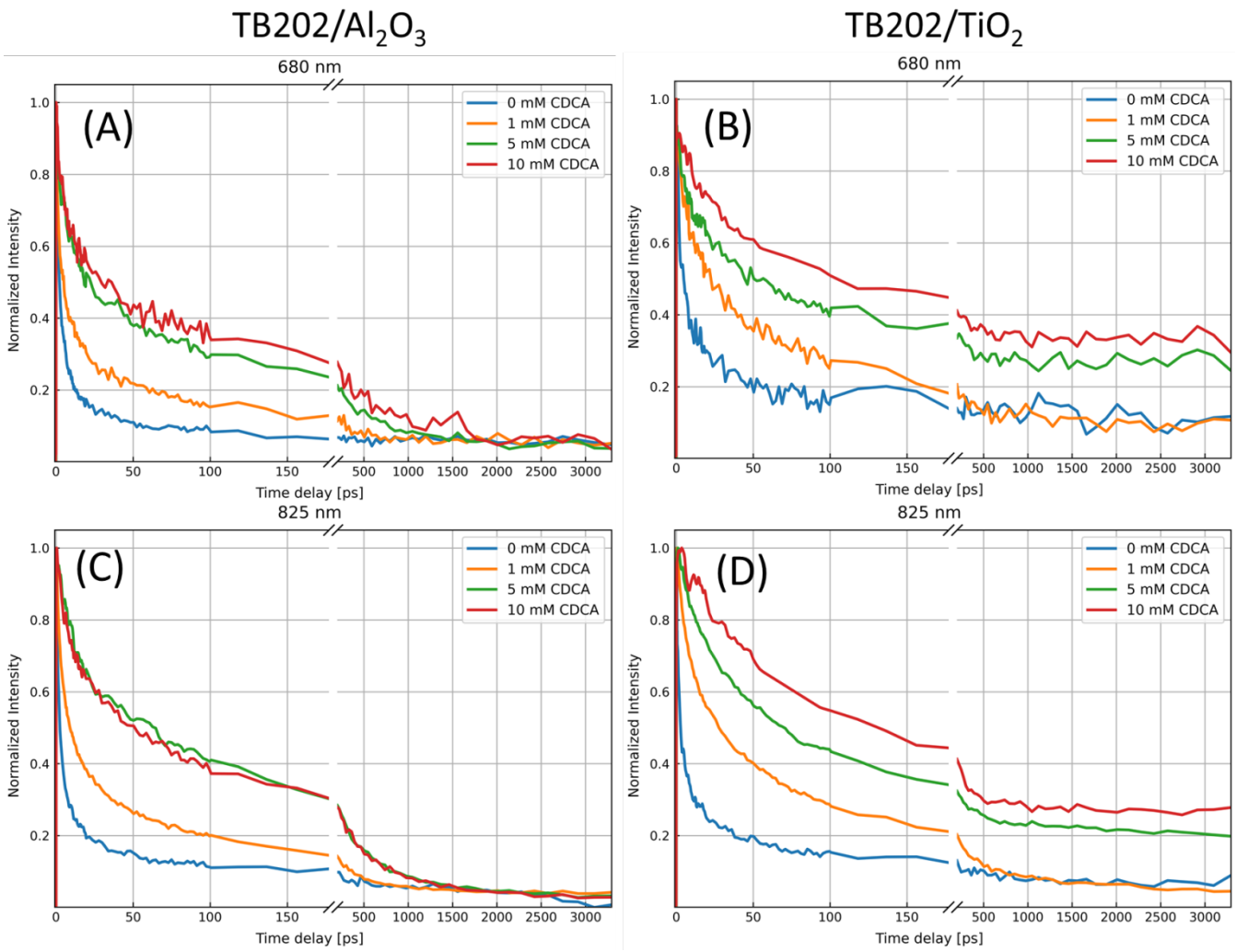

Figure S12. Normalized kinetic traces of TAS data for TB202/Al_2O_3 (A,C) and TB202/TiO_2 (B,D) cells with different CDCA concentrations as indicated on the plot averaged at 680 nm(A,B) and 825 nm (C,D) wavelengths. The 680 nm wavelength corresponds to the ESA signal at short-times, which later decays into the excited aggregate and the cation spectra. The 825 nm is a wavelength where there is GSB and SE signal. These kinetics shows photoproduct formation for TiO_2, which we identify as the cation resulting from CT. The cation spectral signature increase at higher CDCA, with the decrease of the aggregation.

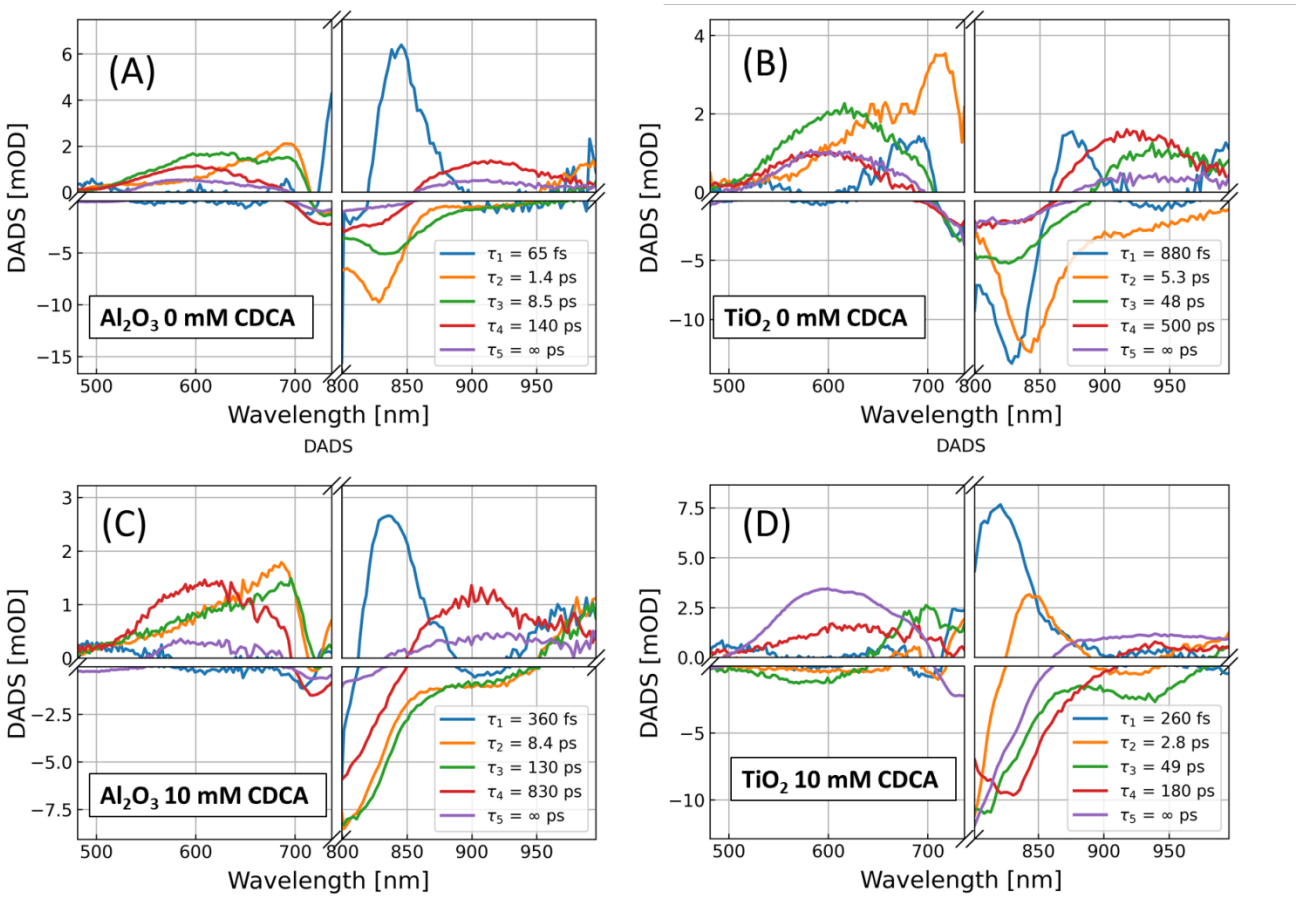

Figure S13. Decay-associated differential spectra of TB202/TiO_2 0 mM CDCA (A) TB202/Al_2O_3 0 mM CDCA (B) TB202/TiO_2 10 mM CDCA (C) TB202/Al_2O_3 10 mM CDCA (D). The spectral shape of the DADS corresponding to τ_2 is similar in (A-C), which corresponds to vibrational relaxation of the excited state. The τ_4 component on plot on D is reminiscent to the spectra of the excited aggregate resulting from ET in Al_2O_3 cells. The last infinite lifetime on plot D component represents the cation spectrum a round "bump" between 500 and 700 nm and a flat spectra >870 nm.

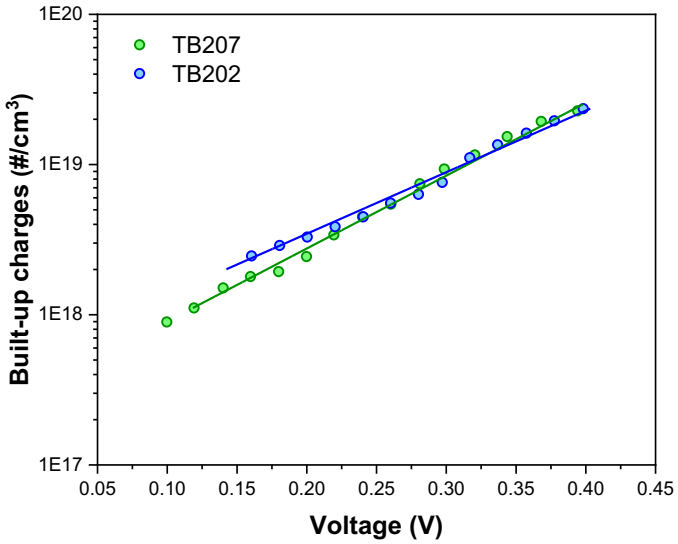

Figure S14. Charge extraction experiments performed for both dyes on TiO_2 devices with 50 mM CDCA: built-up charge density as a function of the bias voltage. The equality of the built-up densities shows that the distribution of density of states and the energetics of the TiO_2 conduction band edge is the same and not affected by the chemical composition of the two dyes.

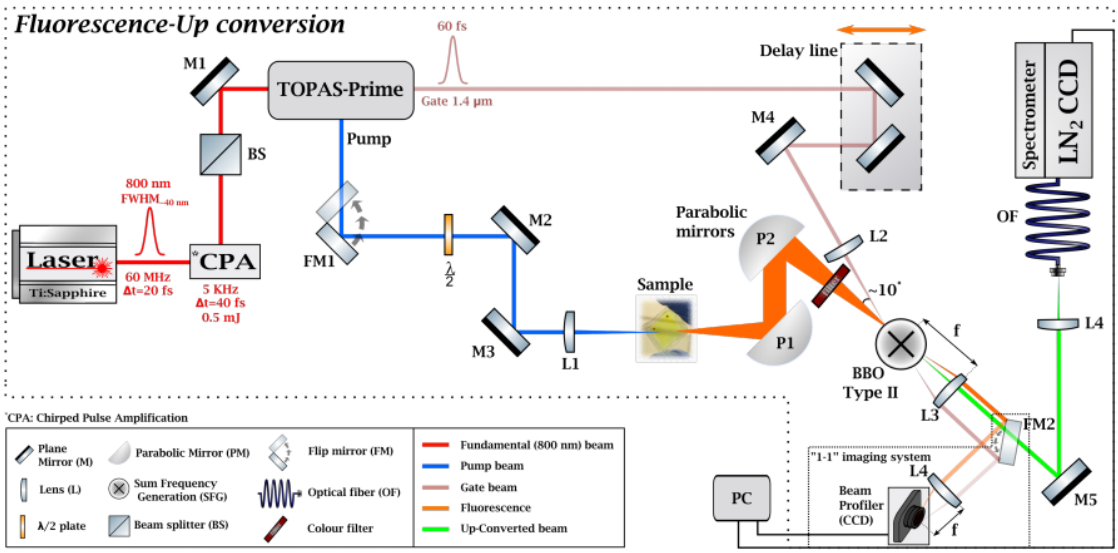

Figure S15. Sematic graph of the fluorescence up-conversion setup. [48]

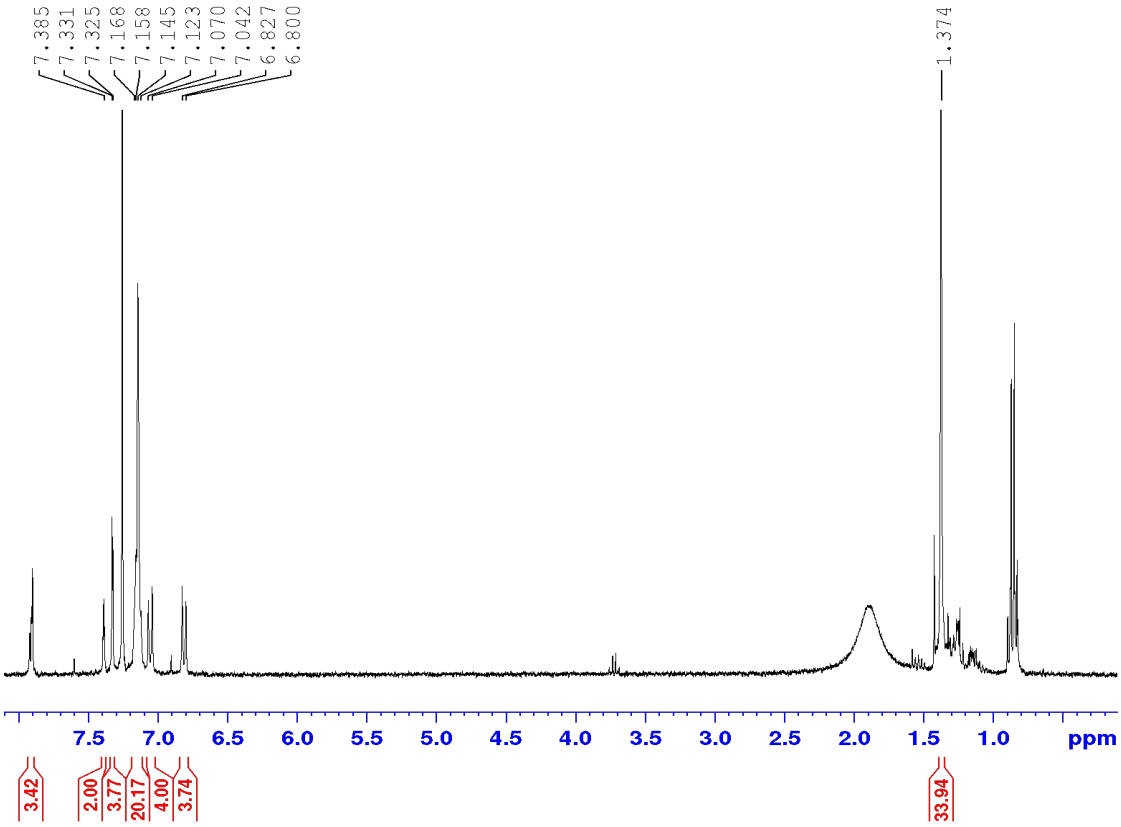

Figure S16. ^{1}H NMR spectrum of compound **TB207**.

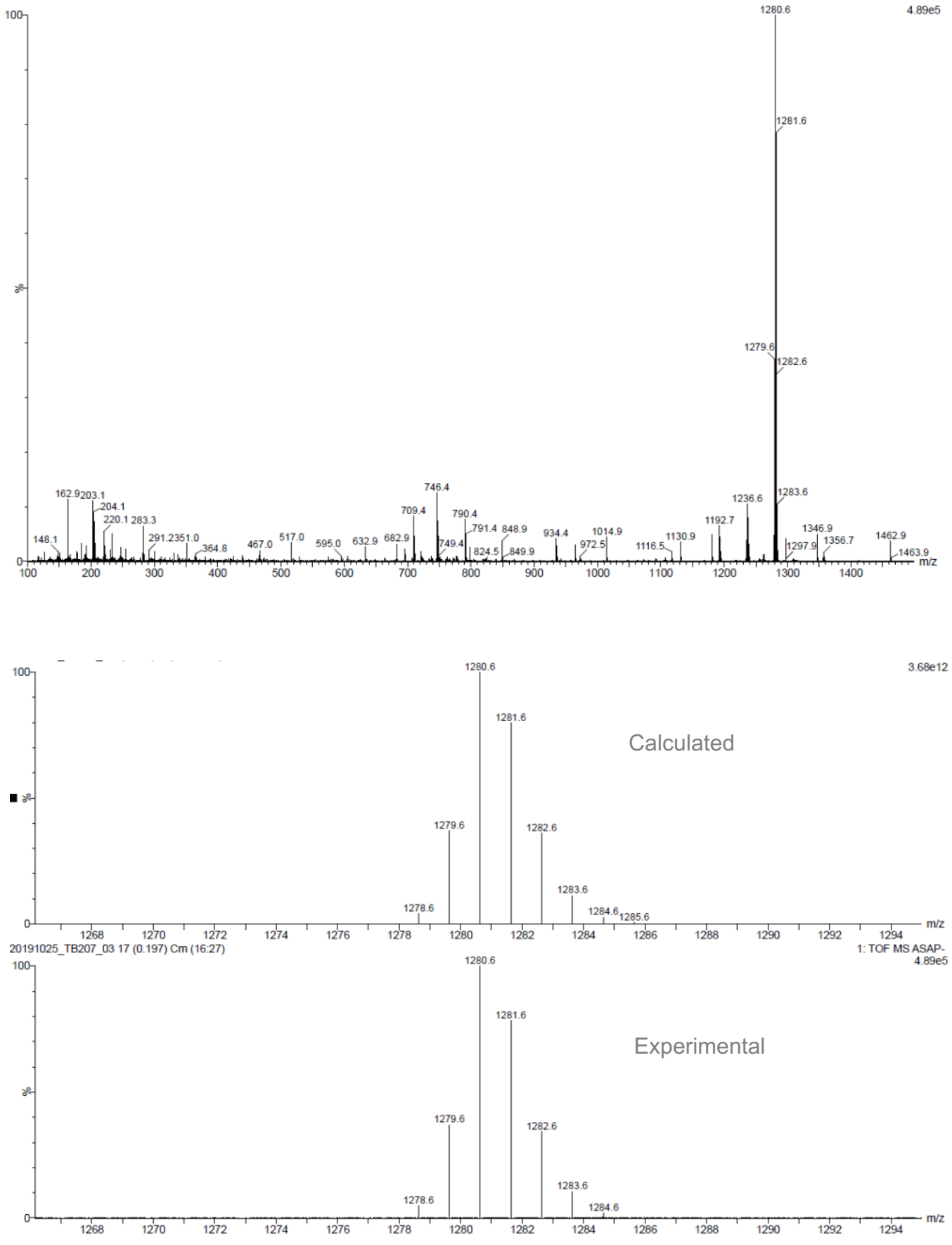

Figure S17. MALDI-TOF spectrum of compound **TB207**. Entire experimental spectrum (top) and superimposition of the simulated and experimental molecular fragment (bottom).

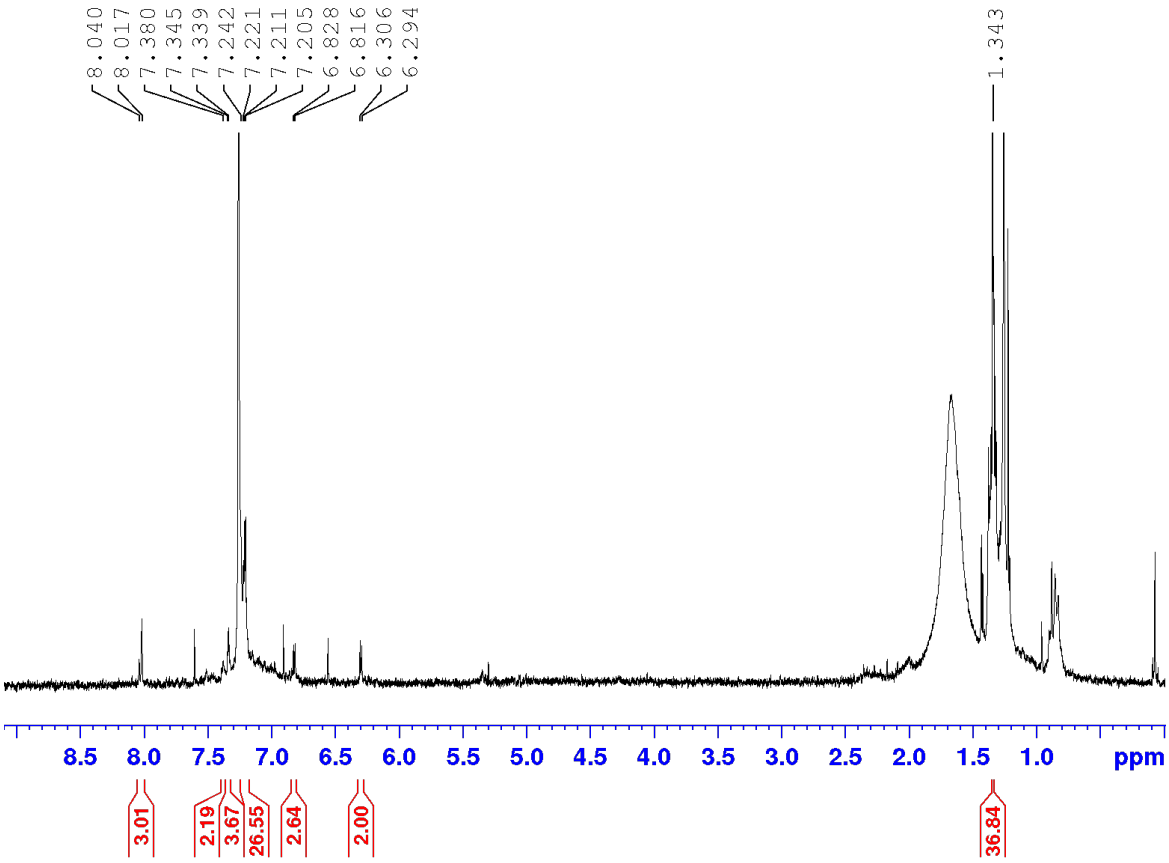

Figure S18. ^{1}H NMR of compound **TB202** recorded in $CDCl_3/CD_3OD$: 9/1.

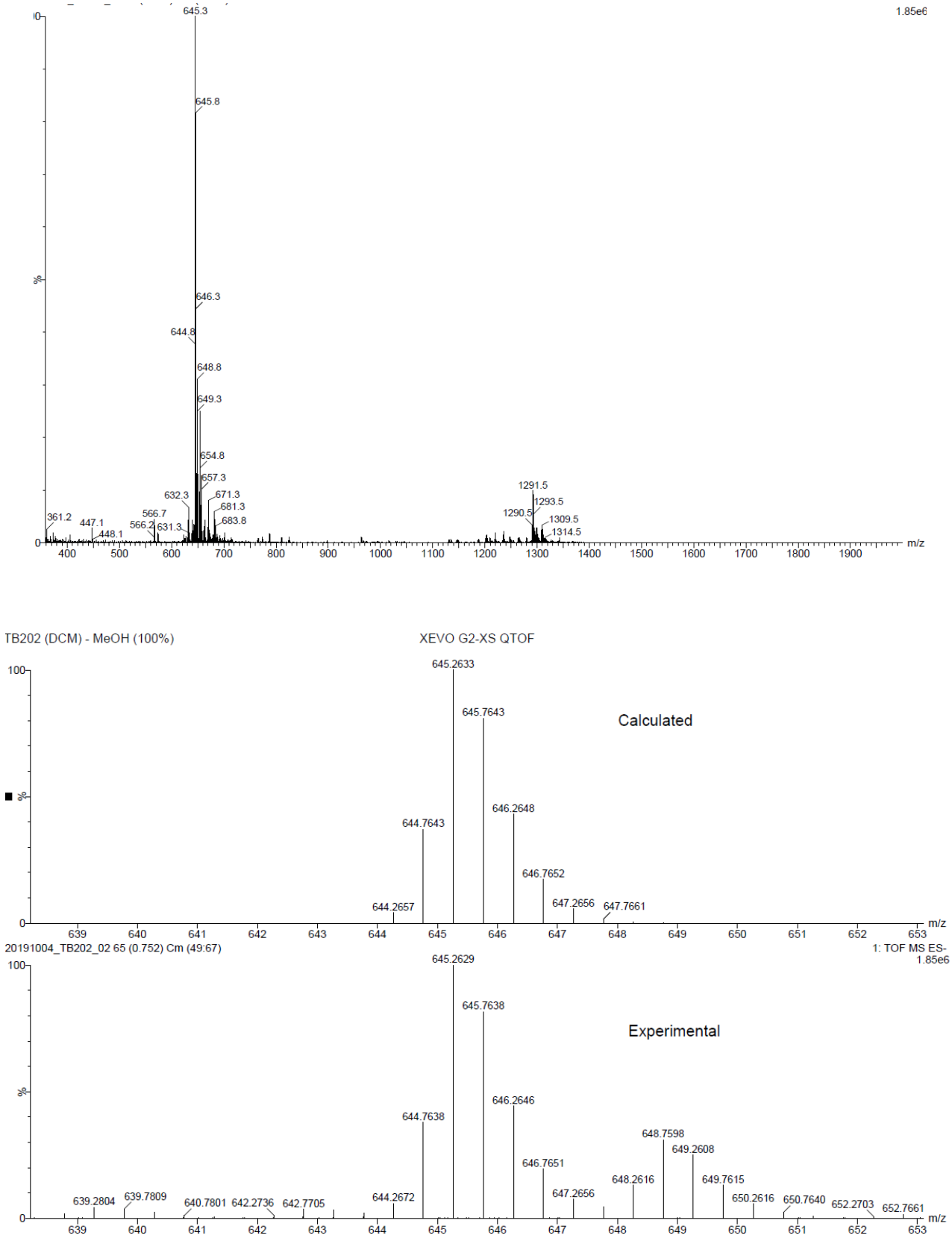

Figure S19. MALDI-TOF spectrum of compound **TB202**. Entire experimental spectrum (top) and superimposition of the simulated and experimental molecular fragment (bottom).

2) The aggregation model: Determining the inter-monomer distance and tilt angle in dimers

Figure S20 recalls the main results of Kasha's theory for the optical properties of a molecular dimer [18,42] as a function of the main geometric parameters. R is the center-to-center distance, α the tilt angle, and θ the tilt angle between the dipole axis and horizontal axis. interaction energy. J-, H-type and co-planar aggregates have α =0°, and θ changes from 0 to 90° for the aggregates (fig. S20). We treat here the special case of oblique aggregates (θ=0°), which are the most relevant geometries present after grafting on the SC nano-particles. Both transitions are allowed , as observed for all absorption spectra in this paper, and as reported for other dyes studied by us[5,6]. For a given distance R, the electronic coupling $\boldsymbol{V} = \frac{|\vec{\mu}|^2}{\boldsymbol{R^3}}\left(\boldsymbol{cos\alpha - 3cos^2\theta}\right)$ is mainly a function of α. The Davidov splitting $2V$, the splitting between the two aggregate absorption bands, (fig. 5) is in the range of 0.18 – 0.19 eV, similar to what was found for pentamethine cyanines [54,55]. In the oblique arrangement $\boldsymbol{\alpha = \pi - 2\theta}$, which allows to express the ratio of the oscillator strength of the two allowed transitions by $\boldsymbol{f_{low}/f_{high} = tan^2(\alpha/2) = A_{low}/A_{high}}$.[56,57] Here, the f's and A's are respectively the oscillator strengths, and the integrated areas of the absorption bands related to the high and low energy transitions (often referred as to H- and J-transitions).

a

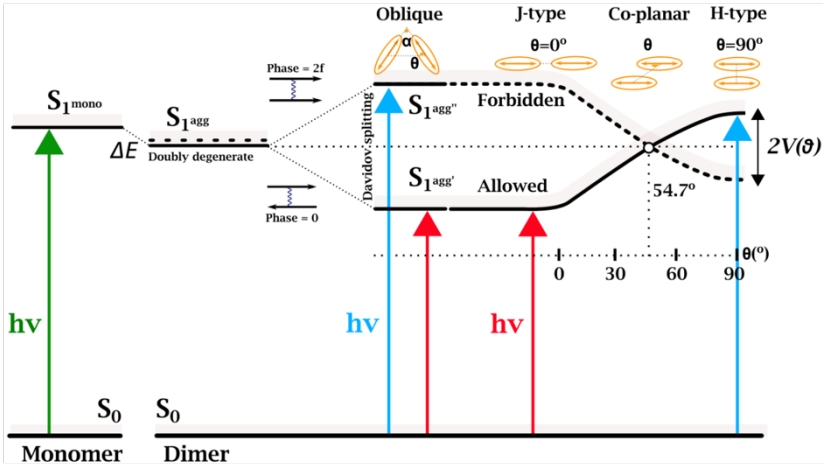

Figure S20: *Schematic of the transition energies of in molecular dimers as a function of their geometrical arrangement. As discussed in the text, the dyes arrange in an oblique fashion after grafting on the semiconductor nanoparticles.*

One can also determine R through the formula[40,57]

$\boldsymbol{R = \left(\frac{185\{cos\alpha + 3sin\frac{\alpha}{2}\}}{V\bar{\nu}} \int_{mono} \varepsilon(\nu) d\nu\right)^{1/3}}$, where $\bar{\nu}$ is the energy of max. absorption of the monomer and $\varepsilon(\nu)$ its molar absorption coefficient.

Based on these relations, we determined the CDCA dependence of R and α, for the TB207/TiO2 devices. The results are summarized in table ST3 below.

CDCA conc.	A_{low}/A_{high}	V (eV)	f_{low}/f_{high}	α (deg)	R (Å)
0 mM	1.25	0.18	0.91	87	18.4
2 mM	1.70	0.18	1.28	97	18.7
5 mM	2.94	0.18	1.95	109	18.7
10 mM	3.13	0.17	1.95	109	19.0

Table ST3: CDCA dependence of R and α, as determined from the dimer-spectra (fig. 5, main text) through the parameters A_{low}/A_{high}, f_{low}/f_{high}, and V.

3) Calculation of the injection efficiency from time-averaged decay rates and based on the modified Kohlrausch decay fitting function

To calculate the injection efficiency we can compare the kinetics of cells for Al_2O_3 and TiO_2, where the aggregation is the same. In the Al_2O_3 cell, where there is only ET, we can express the normalized decay law as follows, with a **time-dependent ET rate.**

$$\frac{dN^*_{Al_2O_3}(t)}{dt} = -k_{ET}(t)N^*_{Al_2O_3}(t) \quad (1)$$

, where N* is number of excited molecules, normalized so that the equation $N^*_{Al_2O_3}(0) = 1$ is true.

In the TiO_2 cell, we have charge transfer as well as ET. The modified decay rate will take the following form

$$\frac{dN^*_{TiO_2}(t)}{dt} = -\left(k_{ET}(t) + k_{CT}(t)\right)N^*_{TiO_2}(t) \quad (2)$$

The change in number of molecules that are subject to ET only can be described similarly.

$$\frac{dN^{ET}_{TiO_2}(t)}{dt} = k_{ET}(t)N^*_{TiO_2}(t) \quad (3)$$

We will assume $k_{ET}(t)$ is the same for the TiO_2 and the Al_2O_3 cell. The number of excited molecules that inject charges, is given by the total number of excited molecules $N^*_{TiO_2}(0)$ minus those "lost" by ET. The injection efficiency is then given by the number of injecting molecules divided by $N^*_{TiO_2}(0)$:

$$\eta_{inj} = \frac{N^*_{TiO_2}(0) - N^{ET}_{TiO_2}(\infty)}{N^*_{TiO_2}(0)} = 1 - N_{ET}(\infty) \quad (4)$$

Based on this equation all the molecules that undergo ET can be expressed by $\int_0^\infty \frac{dN_{ET}}{dt}dt$. Equation (4) then becomes:

$$\eta_{inj} = 1 - \int_0^\infty \frac{dN_{ET}}{dt}dt = 1 - \int_0^\infty k_{ET}(t)N^*_{TiO_2}(t)dt \quad (5)$$

For both the TiO_2 and Al_2O_3 cells we can use the modified Kohlrausch decay function for the fitting.

$$N^*_{TiO_2}(t) = \exp\left(1 - \left(1 + \frac{t}{\tau_{TiO_2}}\right)^{\beta_{TiO_2}}\right) \quad (6)$$

The two fitting parameters for the fitting we determine are β and τ. The k function can be also calculated for Al_2O_3 cell.

$$k_{ET}(t) = \frac{\beta_{Al_2O_3}}{\tau_{Al_2O_3}}\left(1 + \frac{t}{\tau_{Al_2O_3}}\right)^{\beta_{Al_2O_3}-1} \quad (7)$$

Using the functions of equation (6) and (7) the injection rate can be calculated for the modified Kohlrausch decay:

$$\eta_{inj} = 1 - \int_0^{\infty} \frac{\beta_{Al_2O_3}}{\tau_{Al_2O_3}} \left(1 + \frac{t}{\tau_{Al_2O_3}}\right)^{\beta_{Al_2O_3}-1} \exp\left(1 - \left(1 + \frac{t}{\tau_{TiO_2}}\right)^{\beta_{TiO_2}}\right) dt \quad (8)$$

This integral doesn't have an analytical form, but can be evaluated using numerical integration with different β and τ values. We have determined these values using the quad function in the scipy package called in python